Article

Blue Autofluorescence Fundus Imaging for Monitoring Retinal Degeneration in Royal College of Surgeons Rats

Ettel Bubis[1,2], Ifat Sher[1], Alon Skaat[1,2], Inbal Sharvit-Ginon[3,4], Alicja M. Szalapak[5], Iris Moroz[1], Ofra Kalter-Leibovici[2,6], and Ygal Rotenstreich[1,2]

[1] Goldschleger Eye Institute, Sheba Medical Center, Tel-Hashomer, Israel
[2] Sackler Faculty of Medicine, Tel Aviv University, Tel Aviv, Israel
[3] Department of Psychology, Bar Ilan University, Ramat-Gan, Israel
[4] The Joseph Sagol Neuroscience Center at Sheba Medical Center, Israel
[5] St. John's College, University of Cambridge, Cambridge, UK
[6] Unit of Cardiovascular Epidemiology, Gertner Institute for Epidemiology and Health Policy Research, Ramat Gan, Israel

Purpose: Development of a method for noninvasive longitudinal follow-up of retinal degeneration in the whole retina for Royal College of Surgeons (RCS) rats, a commonly used model of retinitis pigmentosa associated with mutations in the MER-proto-oncogene tyrosine kinase (*MERTK*) gene.

Methods: Pigmented RCS rats at postnatal (p) days p28 to p84 were subjected to a biweekly spectral-domain optical coherence tomography (SD-OCT), blue laser fundus autofluorescence (BL-FAF) imaging, and multicolor fundus imaging. Wild-type (WT; Long Evans) rats were tested as control.

Results: Hyperautofluorescence developed throughout the fundus at p42, concomitant with a significant increase in SD-OCT thickness and reflectivity of the debris zone (DZ) layer as well as thinning of the photoreceptor outer nuclear layer (ONL). From p56 to p84, discrete hypofluorescent lesions surrounded by hyperfluorescent flecks were demonstrated around the optic disc that gradually spread throughout the retina. The hypofluorescent lesions were associated with loss of ONL and gradual thinning of the DZ layer. No hypofluorescent BL-FAF lesions were observed in WT rats.

Conclusions: This study suggests that BL-FAF imaging may present a new method for noninvasive longitudinal follow-up of retinal degeneration in nearly the whole retina in RCS rats.

Translational Relevance: A clinical test was developed that may be implemented in translational studies in the RCS rat model of *MERTK*-associated retinitis pigmentosa.

translational vision science & technology

Introduction

Retinitis pigmentosa (RP) is the most common hereditary blinding disease affecting 1 in 4000 to 5000 people worldwide. To date, over 79 causative genes have been reported to be associated with nonsyndromic RP as listed in RetNet.[1] Mutations in these genes lead to rod photoreceptor dysfunction and degeneration that cause night blindness and peripheral visual field loss. At later stages, the dysfunction of photoreceptors in the macula leads to loss of central vision.[2] At least 58 genes have been implicated in autosomal-recessive RP. Most of the genes are rare, causing 1% or fewer cases. One of the more common causative genes for RP is the MER Proto-Oncogene, Tyrosine Kinase (*MERTK*) gene that encodes a transmembrane receptor tyrosine kinase.[3–6] Approximately 3% of autosomal-recessive RP result from mutations in this gene.[7,8] The *MERTK* receptor is expressed in retinal pigment epithelium (RPE) cells where it mediates the phagocytosis of the constantly shed photoreceptor outer segments (POS).[9] In the absence of functional *MERTK*, toxic POS debris accumulate in the subretina and lead to photoreceptor cell death and vision loss, as was first demonstrated in studies in Royal College Surgeons (RCS) rats, that

carry a deletion mutation in the *MERTK* gene.[4] Histologic analyses of these rats demonstrated a buildup of a thick autofluorescent layer containing the nonphagocytosed POS debris in the subretinal space that was termed the debris zone (DZ).[10–13] Optical coherence tomography (OCT) in patients with *MERTK* mutations revealed a similar accumulation of debris in this layer.[5,6] Several studies demonstrated that the strong autofluorescent signal in the DZ layer results from enhanced biosynthesis of bisretinoids in the photoreceptor cells and increased levels of lipofuscin in the retina due to the inadequate clearance of the POS.[14–17] The toxic accumulation of POS debris leads to photoreceptor apoptosis and massive cell loss in the retinal outer nuclear layer (ONL) in patients and in the RCS rat model.[13,18–21]

The RCS rat model has been extensively used in translational studies for testing the potency and safety of new interventions for *MERTK*-associated RP. These include laser photocoagulation,[22] supplementation of the affected *MERTK* gene using viral vectors,[23–27] and cell-based therapies aimed at replacement of the defective RPE cells and restoring POS phagocytosis.[17,28] In 2011, the successful gene therapy translational studies in the RCS rats have led to initiation of a phase I clinical trial with *MERTK*-associated RP patients[29] that is still recruiting patients (NCT01482195), underscoring the translational importance of this rat model. Hence, development of objective noninvasive methods for in vivo longitudinal assessment of retinal degeneration, RPE function, and debris accumulation in the RCS rat model is of major importance. It was recently demonstrated that OCT imaging can be used for monitoring in vivo the changes in retinal layer thickness, including the DZ and ONL in RCS rats.[11,30,31] However, the cross-sectional OCT scans cover up to $30° \times 25°$ and thus can demonstrate only local changes in the scanned area. In order to assess the health of the whole retina, numerous OCT scans would be required that would be extremely laborious and time consuming.

Blue laser fundus autofluorescence (BL-FAF) imaging enables noninvasive longitudinal en face monitoring of the distribution of lipofuscin in RPE cells and bisretinoids in the photoreceptors.[16,32–34] In the last decade, BL-FAF has been used for evaluation of RPE health and disease progression in age related macular degeneration (AMD) patients as well as in RP patients, including RP patients with mutations in the *MERTK* gene.[5,35–38]

In the presented study, we developed a method for noninvasive longitudinal assessment of retinal degen-eration in the whole retina of RCS rats using BL-FAF imaging and quantification of hypofluorescent areas. BL-FAF imaging illustrated changes in the DZ that were associated with progression of photoreceptor degeneration, suggesting that BL-FAF may present an additional modality for in vivo longitudinal assessment of disease progression in RCS rats.

Methods

Animals

Twenty-one pigmented RCS rats[39] and seven Long Evans rats were used in this study. Rats were born and bred in the Sheba Medical Center animal facility under dim cyclic light (12 hours at <5 lux, 12 hours in the dark). All animal procedures and experiments were conducted with approval and under the super-vision of the Institutional Animal Care Committee at the Sheba Medical Center, Tel-Hashomer, and conformed to recommendations of the ARVO State-ment for the Use of Animals in Ophthalmic and Vision Research.

SD-OCT, BL-FAF, and Multicolor Fundus Imaging

Animals were anesthetized using a ketamine (75 mg/kg; Vetoquinol, Lure, France) and xylazine (10 mg/kg; Eurovet Animal Health, Bladel, The Nether-lands) mixture injected intraperitoneally. Eyes were further numbed with a 0.4% oxybuprocaine hydro-chloride solution (Localin; Fischer Pharmaceutical Labs Ltd., Tel Aviv, Israel) and pupils were dilated using a 0.5% tropicamide solution (Midramid; Fischer Pharmaceutical Labs Ltd.). A powerless contact lens (Polymethyl methacrylate) 2.70/5.20, radius of curvature of the central optic zone: 2.70 mm; diameter: 5.20 mm; Cantor & Nissel, Brackley, UK) was placed on the eye and the eye lashes were gently brushed away. All scans were performed using a Heidelberg Spectralis confocal scanning laser ophthalmoscope (Heidelberg Engineering, Heidel-berg, Germany). A blue laser diode with wavelength 486 nm was used to excite the intrinsic autofluores-cence. A barrier filter at 500-nm separated excitation and fluorescence light.

Heidelberg Spectralis SD-OCT was used employ-ing TruTrack active eye tracking and AutoRescan procedures for rescanning at the exact same location of the retina as the baseline examinations.

We used a set of 1536 consecutive A-scans for each

B-scan. The A-scan ("depth scan") is the OCT signal recorded by the detector during a complete travel of the reference mirror. The OCT image (B-scan) is generated by moving the sample beam across the sample surface with an A-scan being recorded at each position of the beam.[40]

To improve the quality of the data and reduce noise, 50 B scans of the same position were averaged in a single OCT image. Twenty-five averaged images spaced 153 μm from each other were used to visualize an area of 5.4 × 3.6 mm.

BL-FAF Scanning

BL-FAF scanning was performed using a 30° lens. First, the optic disc and the blood vessels were used as an alignment target in the infrared (IR) scan mode. Then, the platform was switched to BL-FAF scanning mode and the focus was adjusted for maximum clarity of the vessels. When a clear picture was obtained, the lighting setting was adjusted manually to eliminate overexposure as much as possible without losing the contour of blood vessels. Supplementary Figure S1 illustrates a representative BL-FAF scan at maximal exposure settings (panel A) and the scan at a lower light intensity used for this study (panel B). In order to obtain a spectral-domain (SD) OCT scan of individual lesions, the length of the reference arm was manually adjusted upon achieving a sharp BL-FAF image, following manufacturer's instructions. To obtain BL-FAF images of nearly the entire retina, the optic disc was positioned at the center of the first image (Supplementary Fig. S2A). For imaging of the superior, inferior, nasal, and temporal regions, imaging was performed by placing the camera so that the optic disc was located at the periphery of the frame at the appropriate position as shown in Supplementary Figures S2B to S2E. Because automatic image registration (the AutoRescan function) is not available for fundus imaging in the Spectralis platform, BL-FAF scans were re-scanned in follow-up testing using the position of the optic disc and blood vessels for orientation.

Multicolor Fundus Imaging

Multicolor fundus imaging was preformed following each BL-FAF scan, capturing the same area using the angle and focus settings applied for the BL-FAF scan but manually adjusting the lighting settings for maximum clarity. Because the AutoRescan function is only available for OCT imaging, this technique was used to maintain consistency of acquisition.

BL-FAF Hypofluorescence Quantification

The Region Finder tool (Heidelberg Engineering) was used to measure the hypofluorescent area. This software tool automatically aligns all scans taken from the same area at different time points. All scans were measured while applying preset picture parameters (shadow correction-9 pixels; smooth-3 pixels), minimal small vessel detection threshold (10 μM), maximum large vessel detection threshold (200 μM), and maximum bootstrap settings (98%). The "region growth limit" parameter was kept at 100% and the "region growth power" parameter was manually adjusted to mark the hypofluorescent region as demonstrated in Supplementary Figures S1 and S3. Block lines (short straight red lines in Supplementary Fig. S1) were used to block-out blood vessels when automatic settings were insufficient. Semiautomatic quantification of the hypofluorescent area in BL-FAF images was performed by two independent readers with different degrees of experience (a senior ophthalmologist [AS] and a PhD student [EB]), using Region Finder software (version 26.2.0; Heidelberg Engineering) following manufacturer instructions. Data are presented as the percentage of scanned area covered by the hypofluorescent spots (mean of both eyes and of the two readers). For quantification of the hypofluorescent area in BL-FAF images of the central retina we used scans that were centered on the optic disc, as shown in Supplementary Figures S3A to S3C. The images had a resolution of 1536 × 1536 pixels (30° frame). The percentage of hypofluorescent area out of the total area of the image was calculated. For the superior and inferior quadrant measurements, we used scans in which the optic disc was set at the bottom or top of the scan, respectively, as shown in Supplementary Figures S3D to S3F. The hypofluorescent area was measured within a designated trapezoid defined by three adjacent blood vessels (red lines, Supplementary Figs. S3E, S3F) with height of 5 mm from the edge of the optic disc (highlighted by a yellow line in Supplementary Fig. S3E). The percentage of hypofluorescent area out of the total area of the trapezoid was calculated. All data are presented as binocular mean measured by the two readers.

Currently, the Heidelberg BL-FAF imaging platform does not allow for signal intensity standardization in rodents. Therefore, the outcome measure used in this study was the percentage of hypofluorescent area and the indication of hypofluorescent and hyperfluorescent only refers to relative levels in the

same image. Nevertheless, the illumination settings do not significantly affect the measurement of hypo-fluorescent area, as shown in Supplementary Figure S1.

SD-OCT Segmentation and Measurements

Measurements of retinal layer thicknesses were taken from a 1.4- to 2.4-mm area around the optic disc at the indicated time points. SD-OCT scans were exported from the device as AVI files and analyzed using ImageJ (Fiji) version 1.51a (National Institutes of Health, Bethesda, MD). Segmentation was manually performed in a strict perpendicular angel as shown in Supplementary Figure S4. A template was devised to ensure that the measurements were always taken from an area of 1.4 to 2.4 mm away from the optic disc, sampling four quadrants of the retina. The template was overlaid on top of the scans and used to delineate the appropriate areas for measurement (as illustrated in Supplementary Fig. S4). Total retina, ONL and DZ thicknesses were averaged from four quadrants for each eye in each time point in each quadrant. Because other studies reported that there was no difference in the progression of retinal degeneration between left and right eyes in these rats,[31] the values are presented as the mean of both eyes. All measurements were performed by two observers (EB and AMS).

Histology

Eyes from 21 RCS rats were removed for histology analysis at the appropriate time points (postnatal day [p]28: $n = 3$; p42: $n = 3$, p56: $n = 3$; p70: $n = 3$; p84: $n = 9$). Eyes were fixed in formalin, embedded in paraffin, and 4-μm sections were cut along the vertical meridian of the eye through the optic nerve. Sections were stained with hematoxylin and eosin and were visualized and photographed by light microscopy (Olympus BX51, Hamburg, Germany).

Statistical Analysis

Statistical analyses were performed using SPSS software (IBM SPSS Statistics 20 for windows, IBM Corp., Armonk, NY). To test the within-subjects effect of the percentage of hypofluorescent area in central retina measured in different time points, we used the univariate generalized linear models for repeated measures. To test the within-subjects effect of the percentage of hypofluorescent area in inferior and superior regions measured simultaneously in these time points, we used a doubly multivariate

repeated measures design within this model. The Bonferroni test was used to correct for multiple comparisons in post hoc analyses.

The agreement between the two observers was tested, following the method of Altman and Bland.[41] We plotted the difference between the paired measurements against the mean value of these measurements, and tested the correlation coefficient against the null hypothesis of $r = 0$. The mean differences in interobserver agreements were 0.73 mm^2 and −0.17, 0.08, and −0.06 μm for BL-FAF area and SD-OCT thickness of ONL, DZ, and total retina, respectively, with no significant difference between readers (Supplementary Fig. S5). There was no evidence that the difference between the two observers changed with the magnitude of the measurements ($P > 0.8$ for all bivariate correlation coefficients).

Results

BL-FAF Longitudinal Follow-Up

Figures 1A to 1E demonstrate a representative longitudinal BL-FAF follow-up of an RCS rat at ages p28 to p84. Longitudinal BL-FAF follow-up of additional rats are shown in Supplementary Figure S6. At p28, the BL-FAF signal was weak throughout the posterior pole, even though the image was acquired using the highest illumination setting available (Figs. 1B–E). At p42 the rats presented an increased BL-FAF signal throughout the fundus. At p56, a hypofluorescent ring was clearly visible around the optic disc in all animals. By p70 all animals presented well-defined hypofluorescent discrete lesions with irregular shapes (black arrows in Figs. 1C, 1D) surrounded by a ring of hyperfluorescent flecks (white arrows in Figs. 1C, 1D). In one animal these lesions were detected as early as p42. Seven animals exhibited these lesions at p56 and one animal presented these lesions only at p84. In addition, starting at p56 the hyperfluorescence was gradually replaced by dark spots of hypofluorescence starting from the inferior retina and gradually spreading to the peripheral, nasal, and temporal retina, mostly sparing the superior retina (Figs. 1C, 1D) until p70. At p84 the hyperfluorescent spots were spread throughout the fundus (Fig. 1E). By contrast, no BL-FAF hypofluorescence was observed in wild-type (WT; Long Evans) rats tested either at a young age (p28) or at p113 (Figs. 1F, 1G).
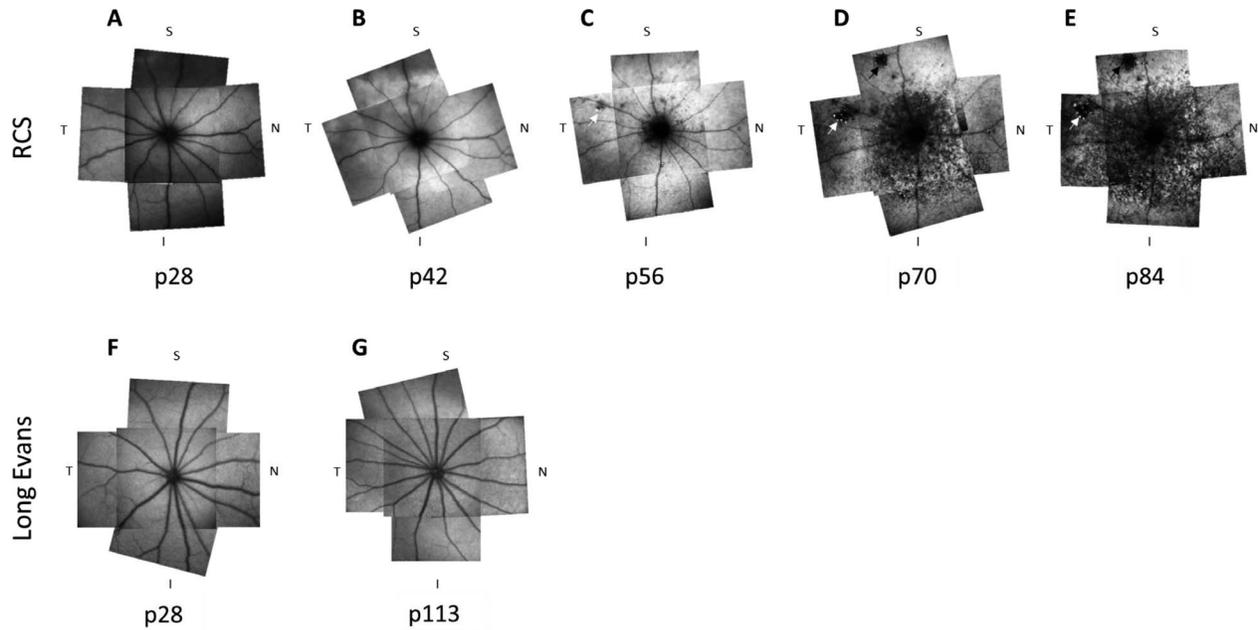
Figure 1. BL-FAF longitudinal follow-up in a representative RCS rat. BL-FAF imaging was performed at indicated days postnatal in a representative RCS rat (A–E). Each *panel* is a composite of five BL-FAF scans. To generate the composite image, the size of the optic disc was matched and then the images were aligned according to the blood vessel orientation. An ImageJ plugin ("Align images by line Region of Interest [ROI]") was used to align the composite images. (F, G) BL-FAF scans of two representative Long Evans rats at ages p28 (F) and p113 (G). T, temporal; N, nasal; S, superior; I, inferior.

Assessment of BL-FAF Hypofluorescent Area

The relative area of BL-FAF hypofluorescence was assessed by measuring the percentage of the area covered by the hypofluorescent spots in the central, superior and inferior retina. Figure 2A demonstrates the increase in the hypofluorescent area within the central retina in aging rats. Nearly 23% of the central retina contained hypofluorescent lesions at p56 and at p70 nearly 70% of the central retina contained hypofluorescent lesions. At p84 both hyperfluorescent and hypofluorescent spots were spread throughout the fundus. The overall within-subjects effect for the hypofluorescent area in different time points was
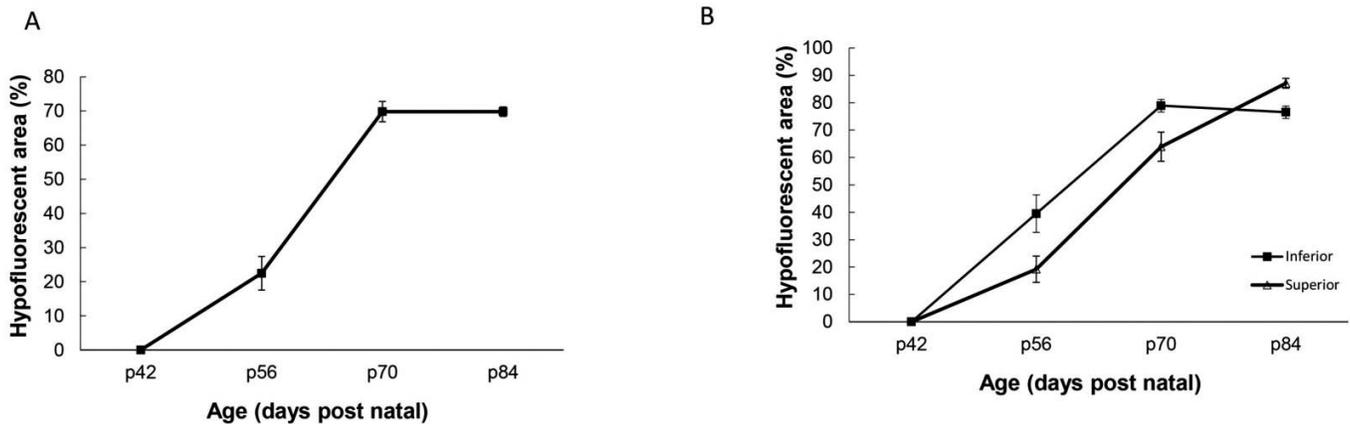

Figure 2. Quantification BL-FAF hypofluorescence in different retinal regions. (A) Increase in BL-FAF hypofluorescent area in the central retina with age. Data are presented as the mean $\pm$ standard error (SE) from 9 rats. (B) Increase in BL-FAF hypofluorescent area in the inferior and superior with age. Percentage of hypofluorescent area was calculated from a trapezoid located superior or inferior to the optic disc, as indicated in the Methods section. Data are presented as the mean $\pm$ SE from the same nine rats used in *panel A*. Hypofluorescence was significantly higher in inferior compared with superior retina at p70 ($P < 0.0001$) and p84 ($P = 0.012$).
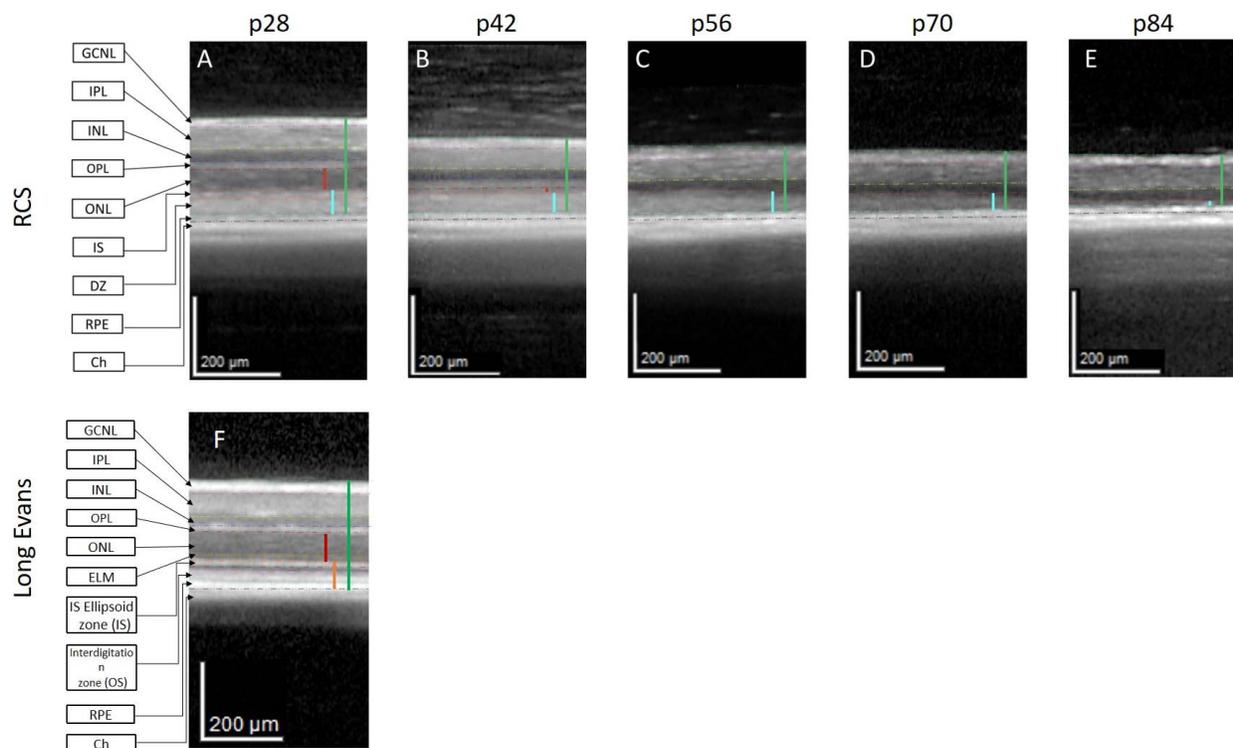
Figure 3. Identification of photoreceptor loss and reduction in DZ layer thickness in RCS rats by SD-OCT. (A–E) SD-OCT scans of the central retina area in a single-representative RCS rat at different ages (p28–p84). (F) A representative SD-OCT scan of WT Long Evans rat at p28. *Vertical lines* highlight the ONL (*red*) and total retina (*green*). The *turquoise vertical lines* indicate the DZ in the RCS rat (A–E). The *orange vertical line* indicates the photoreceptor outer segment layers in Long Evans rats (F). *Horizontal lines* highlight the GCNL, ganglion nerve fiber layer (*green-pink*); IPL, inner plexiform layer (*pink-yellow*); INL, inner nuclear layer (*yellow-blue*); OPL, outer plexiform layer (*blue-magenta*); ONL (*magenta-red*); IS, inner segments (*red-orange*); DZ (*orange-turquoise*); RPE (*turquoise-black*); Ch, Choroid.

significant ($P < 0.0001$). The hypofluorescent area was significantly larger at p56 compared with p42 ($P = 0.011$). While the measurements of hypofluorescent area at the p70 and p84 did not differ significantly, they both differed from the measurement at p42 and p56 ($P < 0.0001$).

As shown in Figures 1, 2B, and Supplementary Figure S6, the hypofluorescent area spread faster in the inferior retina as compared with the superior retina. Thus, at p70 nearly the entire inferior retina was hypofluorescent, whereas only 40% of the superior area was hypofluorescent at this age. The overall within-subjects effects of hypofluorescent area at inferior and superior retina measured at the same time points and tested simultaneously in the model were significant ($P < 0.001$ for both effects). While the measurements of the hypofluorescent area in the inferior retina at the p70 and p84 did not differ significantly, they both differed from the measurement at p56 ($P < 0.001$). All post hoc comparisons for the measurements across time for the hypofluorescent area at the superior retina were statistically significant

($P < 0.001$ for the comparisons of p70 and p84 versus p56, and $P = 0.025$ for the comparison between p70 and p84).

Changes in SD-OCT Retinal Layer Thicknesses

To determine the degenerative process underlying the changes in BL-FAF, SD-OCT imaging was performed. Representative SD-OCT scans of the central retina in a single RCS rat are shown in Figure 3. Scans were taken from the same area in the central retina at each time point using the AutoRescan procedures that enables rescanning at the exact same location of the retina as the baseline examination (Figs. 3A–E). Photoreceptor degeneration was clearly demonstrated by the significant thinning of the ONL at p42 compared with p28 (14.5 ± 0.7 vs. 49.8 ± 0.8 μm, $P < 0.0001$, Table). By p56 the ONL was no longer detectable. At p28 a hyperreflective layer between the ONL and RPE was demonstrated. This layer reflects the DZ, as was demonstrated by Adachi et al.[30] and Ryals et al.[31] This layer was absent in SD-

Table. SD-OCT Retinal Layer Measurements

Age	ONL, μm	DZ, μm	TR, μm
p28	50.5 ± 0.8	51.7 ± 0.8	232.5 ± 2.8
p42	15.3 ± 0.7	44.4 ± 0.6	193.6 ± 1.7
	($p_{28} < 0.0001$)	($p_{28} < 0.0001$)	($p_{28} < 0.0001$)
p56	0.0 ± 0.0	36.6 ± 1.0	175.8 ± 1.5
	($p_{28} < 0.0001$, $p_{42} < 0.0001$)	($p_{28} < 0.0001$, $p_{42} = 0.005$)	($p_{28} < 0.0001$, $p_{42} < 0.0001$)
p70	0.0 ± 0.0	28.6 ± 1.0	163.7 ± 1.8
	($p_{28} < 0.0001$, $p_{56} < 0.0001$)	($p_{28} > 0.0001$, $p_{56} = 0.001$)	($p_{28} < 0.0001$, $p_{56} = 0.001$)
p84	0.0 ± 0.0	15.66 ± 1.6	150.7 ± 0.8
	($p_{28} < 0.0001$, $p_{70} < 0.0001$)	($p_{28} > 0.0001$, $p_{70} \leq 0.0001$)	($p_{28} < 0.0001$, $p_{70} = 0.004$)

The thickness of ONL, DZ, and total retina (TR) was measured in SD-OCT scans of the central retina at the indicated ages as described in the "Materials and Methods" section. Data are presented as the mean ± SE. A one-way repeated-measures analysis of variance with Bonfferoni adjustment with the within-subject factor age (days postnatal) was used to compare between retinal measurements at each time point compared with baseline measurements at p28 or the preceding time point as indicated in subscript.

OCT scans of WT (Long Evans) rats (Fig. 3F). The DZ layer in RCS rats gradually became thinner reaching 16.0 ± 1.9 μm at p84. These findings suggest that the initial increase in the autofluorescent signal occurs in parallel to the marked decrease in ONL and the subsequent hypofluorescence corresponded to the loss of DZ in the SD-OCT scans.

The focal discrete hypofluorescent lesions corresponded to a focal loss of the DZ, as can be seen in Figure 5, while the hyperfluorescent foci surrounding them corresponded to small hyperreflective structures adjacent to the RPE (indicated by colored arrowheads).

The degenerative changes observed in the BL-FAF and OCT imaging were also demonstrated by histologic analysis. The ONL became thinner with aging, correlating with thinning of the hyporeflective ONL layer in the OCT as shown in Figure 4 (blue arrows). At p56, the ONL was reduced to a single-cell layer by histologic analysis (Fig. 4F) and was indistinguishable from the DZ and inner plexiform layers on SD-OCT scans. The DZ was clearly seen in the retinal sections and OCT imaging up to p84 (Fig. 4, white arrows). At p84 the histologic analysis demonstrated a highly disorganized, thin, and heterogeneous DZ layer, correlating with the significant thinning of this layer in the SD-OCT images (Figs. 4I, 4J).

Multicolor Fundus Imaging of RCS Rats

Next, we examined the potential use of multicolor fundus imaging for en face monitoring of retinal degeneration. Figure 6 demonstrates the retinal changes detected by multicolor fundus imaging and by IR fundus scanning compared with the BL-FAF in a representative rat.

Starting at p56, the discrete hypofluorescent lesions that were clearly seen using BL-FAF, could be detected by the green and blue reflection channels and the multicolor imaging as dark lesions (Figs. 6A–U, highlighted with red arrows). These lesions were undetected by IR fundus imaging until p84 (Fig. 6Z, highlighted by a red arrow). The hypofluorescent spots that were clearly demonstrated throughout the fundus in the BL-FAF imaging starting at p56, were nearly undetectable by the other fundus imaging modalities.

Discussion

BL-FAF imaging is commonly used in the clinic for monitoring posterior pole diseases, such as retinal and macular degeneration, inflammation, and malignancies.[37] Here, we developed a readily accessible method to assess retinal degeneration in vivo in the whole retina of RCS rats using BL-FAF imaging.

The retinal degeneration process of these rats initially manifested in the form of an increase of the hyperfluorescent signal throughout the posterior pole at p42. The hyperfluorescent signal was then gradually replaced by hypofluorescent spots until p84, spreading from the inferior retina to the nasal and temporal regions, sparing the superior retina. These BL-FAF changes corresponded with changes in the thickness of ONL and DZ as determined by SD-OCT. At the early age of p28 the ONL layer and a thick DZ
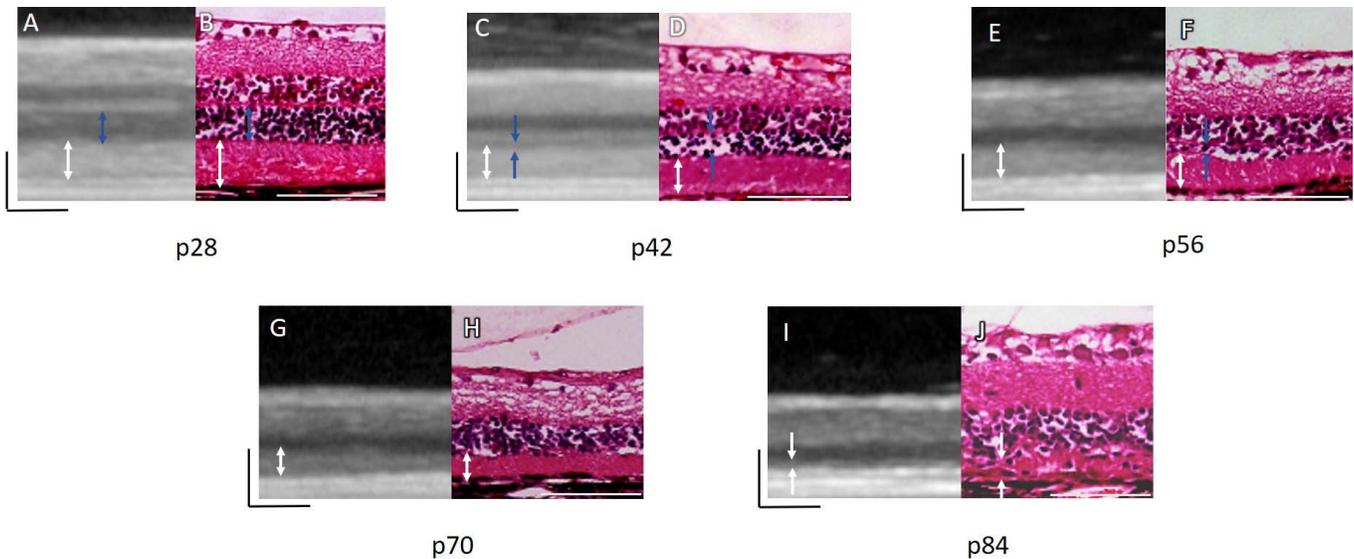
Figure 4. Changes in retinal layers during RCS rat retinal degeneration observed using SD-OCT and the corresponding histological retinal sections. *Blue arrows* indicate the ONL. *White arrows* indicate the DZ. The *black* and *white bars*, 100 μm.

layer were clearly visible on the SD-OCT scans, reflecting poor clearance of POS that most likely led to the increased BL-FAF due to an increase in accumulation of bisretinoids and lipofuscin. At later stages of retinal degeneration, loss of photoreceptors presented as loss of SD-OCT ONL thickness. Subsequently, bisretinoid accumulation was most likely reduced. Eventually the DZ layer became thinner, leading to a patchy loss of BL-FAF signal. These imaging findings are in accordance with our histologic analysis (Fig. 4), histologic analyses per-

formed by others and with studies on biochemical characterization of retinal bisretinoids and stem cell rescue studies in these rats.[13,15,17,42] The BL-FAF imaging enables to assess these degenerative processes in nearly the whole retina by using only five scans total that can be merged into a single mosaic image. Future studies will be aimed at evaluating the potential use of BL-FAF for assessment of the safety and potency of novel treatments for *MERTK*-associated RP in RCS rats. It remains to be elucidated whether this method can be applied in other rodent
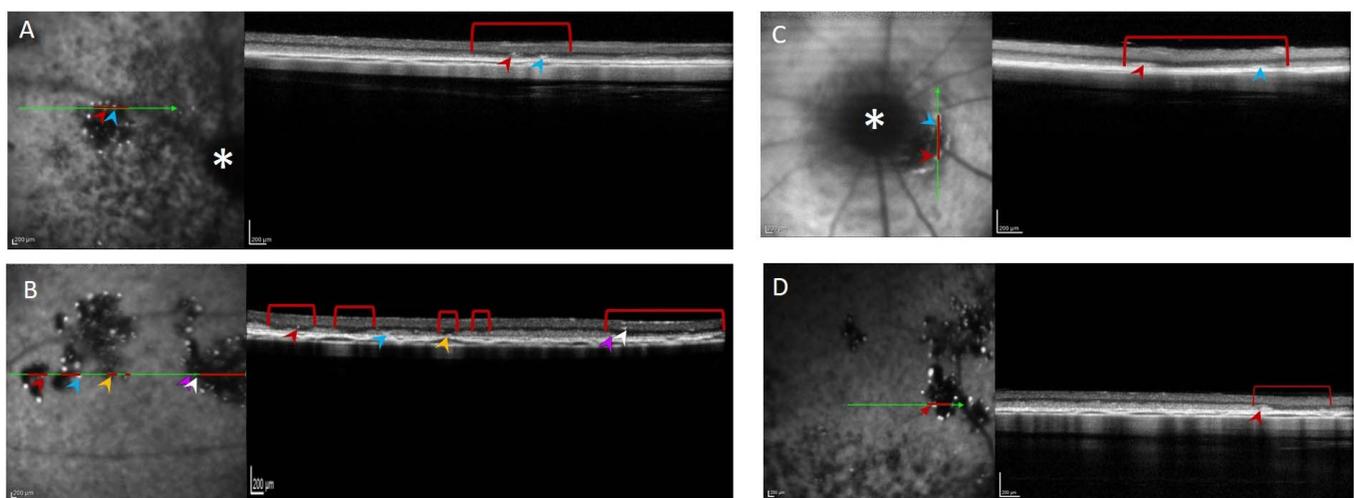

Figure 5. BL-FAF imaging and corresponding SD-OCT scans of well-defined hypofluorescent lesions and hyperfluorescent foci. Lesions detected in animals at p56 (A), p70 (B, C), and p84 (D). The *green arrows* indicate the position from which the SD-OCT scans on the *right* were taken. *Red lines* highlight the lesion cross-sections. The optic disc is marked with a *white asterisk* in (A, C). Hypofluorescent foci are highlighted by *colored arrowheads*.
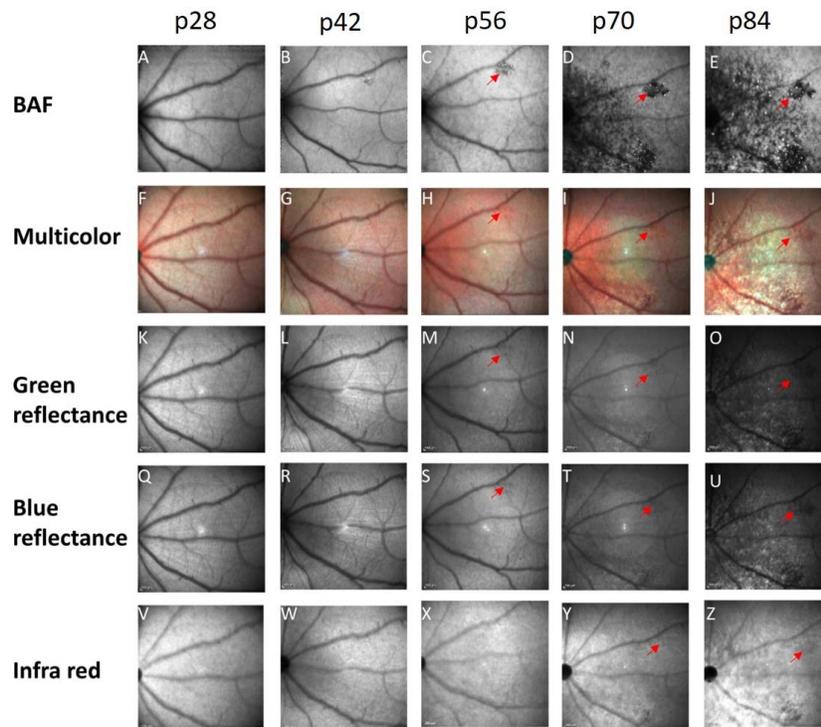
translational vision science & technology

Figure 6. Comparison between different fundus imaging modalities. A representative example of a single-animal follow-up at ages p28 to p84 using BL-FAF (A–E), multicolor fundus imaging (F–J), green reflectance (K–O), blue reflectance (Q–U), and IR fundus imaging (V–Z). A *red arrow* highlights the same hypofluorescent lesion in the different scans.

models for retinal degeneration in which autofluorescent material accumulates within the RPE cells.

This powerful technique enabled us to evaluate the different progression rate of retinal degeneration in superior and inferior retina. Our findings that hypofluorescent lesions spread more slowly in the superior retina compared with the inferior retina are in accordance with histologic analysis published by LaVail et al.[19] and with the recent SD-OCT study by Ryals et al,[31] further supporting our hypothesis that debris accumulating in the DZ and POS are the source of the BL-FAF signal.

Our SD-OCT thickness measurements of total retina and ONL are in good agreement with histologic analysis and measurements of retinal layer thicknesses performed by Ryals et al.[31] even though they were performed using a different SD-OCT device (Ryals et al.[31] used Envisu R2200-HR SD-OCT; Leica Microsystems, Wetzlar, Germany). It is noteworthy that in the present study, retinal thickness was determined using the AutoRescan procedure that enables rescanning at the exact same location of the retina as the baseline examination. This modality increases the accuracy of retinal thickness measurement in longitudinal studies, which is important for accurate

assessment of therapeutic effects and safety in translational studies.

The hypofluorescent spots that were clearly demonstrated in the BL-FAF imaging were nearly undetectable by the other fundus imaging modalities examined, suggesting that the BL-FAF modality is the most sensitive tool for en face assessment of retinal degeneration progression in these rats.

A similar progression of BL-FAF changes was documented in a family with RP due to a splice site mutation c.2189+1G>T in the *MERTK* gene,[5] highlighting the importance of BL-FAF monitoring in RCS rats in translational studies. The youngest sibling in that family (presenting with an early disease stage) demonstrated an increased BL-FAF signal, in accordance with our findings of fundus hyperfluorescence in rats starting at p42. The older siblings presented with patches of decreased BL-FAF surrounded by focally increased BL-FAF that are in accordance with our BL-FAF findings in older rats. These clinical data support our findings in the RCS rat model and suggest that BL-FAF may present a noninvasive, quick, clinically relevant method for longitudinal evaluation retinal degeneration in nearly the whole retina using a few scans. This method may

be useful as a surrogate outcome in translational studies in RCS rats aimed at development of new treatments for *MERTK*-associated RP and may potentially be used in the future in clinical trials with *MERTK*-associated RP patients.

Acknowledgments

References

1. RetNet, retinal information network. Available at: https://Sph.uth.edu/retnet/home.htm. Accessed August 16, 2018.
2. Hartong DT, Berson EL, Dryja TP. Retinitis pigmentosa. *Lancet*. 2006;368:1795–1809.
3. Gal A, Li Y, Thompson DA, et al. Mutations in MERTK, the human orthologue of the RCS rat retinal dystrophy gene, cause retinitis pigmentosa. *Nat Genet*. 2000;26:270–271.
4. D'Cruz PM, Yasumura D, Weir J, et al. Mutation of the receptor tyrosine kinase gene mertk in the retinal dystrophic RCS rat. *Hum Mol Genet*. 2000;9:645–651.
5. Charbel Issa P, Bolz HJ, Ebermann I, Domeier E, Holz FG, Scholl HP. Characterisation of severe rod-cone dystrophy in a consanguineous family with a splice site mutation in the MERTK gene. *Br J Ophthalmol*. 2009;93:920–925.
6. Mackay DS, Henderson RH, Sergouniotis PI, et al. Novel mutations in MERTK associated with childhood onset rod-cone dystrophy. *Mol Vis*. 2010;16:369–377.
7. Abu-Safieh L, Alrashed M, Anazi S, et al. Autozygome-guided exome sequencing in retinal dystrophy patients reveals pathogenetic mutations and novel candidate disease genes. *Genome Res*. 2013;23:236–247.
8. Patel N, Aldahmesh MA, Alkuraya H, et al. Expanding the clinical, allelic, and locus heterogeneity of retinal dystrophies. *Genet Med*. 2016; 18:554.
9. Feng W, Yasumura D, Matthes MT, LaVail MM, Vollrath D. Mertk triggers uptake of photoreceptor outer segments during phagocyto-sis by cultured retinal pigment epithelial cells. *J Biol Chem*. 2002;277:17016–17022.
10. Herron WL, Riegel BW, Myers OE, Rubin ML. Retinal dystrophy in the rat-a pigment epithelial disease. *Invest Ophthalmol Vis Sci*. 1969;8:595–604.
11. Herron WL, Riegel BW, Brennan E, Rubin ML. Retinal dystrophy in the pigmented rat. *Invest Ophthalmol Vis Sci*. 1974;13:87–94.
12. Goldman AI, O'Brien PJ. Phagocytosis in the retinal pigment epithelium of the RCS rat. *Science*. 1978;201:1023–1025.
13. Tzameret A, Sher I, Belkin M, et al. Transplan-tation of human bone marrow mesenchymal stem cells as a thin subretinal layer ameliorates retinal degeneration in a rat model of retinal dystrophy. *Exp Eye Res*. 2014;118:135–144.
14. Katz ML, Eldred GE, Robison WG Jr. Lipofus-cin autofluorescence: evidence for vitamin A involvement in the retina. *Mech Ageing Dev*. 1987;39:81–90.
15. Liu J, Itagaki Y, Ben-Shabat S, Nakanishi K, Sparrow JR. The biosynthesis of A2E, a fluo-rophore of aging retina, involves the formation of the precursor, A2-PE, in the photoreceptor outer segment membrane. *J Biol Chem*. 2000;275: 29354–29360.
16. Sparrow JR, Yoon KD, Wu Y, Yamamoto K. Interpretations of fundus autofluorescence from studies of the bisretinoids of the retina. *Invest Ophthalmol Vis Sci*. 2010;51:4351–4357.
17. Krohne TU, Westenskow PD, Kurihara T, et al. Generation of retinal pigment epithelial cells from small molecules and OCT4 reprogrammed human induced pluripotent stem cells. *Stem Cells Transl Med*. 2012;1:96–109.
18. Dowling JE, Sidman RL. Inherited retinal dystrophy in the rat. *J Cell Biol*. 1962;14:73–109.
19. LaVail MM, Battelle BA. Influence of eye pigmentation and light deprivation on inherited retinal dystrophy in the rat. *Exp Eye Res*. 1975; 21:167–192.
20. Bok D. The retinal pigment epithelium: a versatile partner in vision. *J Cell Sci Suppl*. 1993;17:189–195.
21. Tso MO, Zhang C, Abler AS, et al. Apoptosis leads to photoreceptor degeneration in inherited retinal dystrophy of RCS rats. *Invest Ophthalmol Vis Sci*. 1994;35:2693–2699.
22. Lorach H, Kang S, Dalal R, Bhuckory M, Quan Y, Palanker D. Long-term rescue of photorecep-tors in a rodent model of retinitis pigmentosa associated with MERTK mutation. *Sci Rep*. 2018;8:11312.

23. Vollrath D, Feng W, Duncan JL, et al. Correction of the retinal dystrophy phenotype of the RCS rat by viral gene transfer of mertk. *Proc Natl Acad Sci U S A*. 2001;98:12584–12589.

24. Smith AJ, Schlichtenbrede FC, Tschernutter M, Bainbridge JW, Thrasher AJ, Ali RR. AAV-mediated gene transfer slows photoreceptor loss in the RCS rat model of retinitis pigmentosa. *Mol Ther*. 2003;8:188–195.

25. Tschernutter M, Schlichtenbrede F, Howe S, et al. Long-term preservation of retinal function in the RCS rat model of retinitis pigmentosa following lentivirus-mediated gene therapy. *Gene Ther*. 2005;12:694–701.

26. Deng WT, Dinculescu A, Li Q, et al. Tyrosine-mutant AAV8 delivery of human MERTK provides long-term retinal preservation in RCS rats. *Invest Ophthalmol Vis Sci*. 2012;53:1895–1904.

27. Conlon TJ, Deng W, Erger K, et al. Preclinical potency and safety studies of an AAV2-mediated gene therapy vector for the treatment of MERTK associated retinitis pigmentosa. *Hum Gene Ther Clin Dev*. 2013;24:23–28.

28. Kole C, Klipfel L, Yang Y, et al. Otx2-genetically modified retinal pigment epithelial cells rescue photoreceptors after transplantation. *Mol Ther*. 2018;26:219–237.

29. Ghazi NG, Abboud EB, Nowilaty SR, et al. Treatment of retinitis pigmentosa due to MERTK mutations by ocular subretinal injection of adeno-associated virus gene vector: results of a phase I trial. *Hum Genet*. 2016;135:327–343.

30. Adachi K, Takahashi S, Yamauchi K, Mounai N, Tanabu R, Nakazawa M. Optical coherence tomography of retinal degeneration in royal college of surgeons rats and its correlation with morphology and electroretinography. *PLoS One*. 2016;11:e0162835.

31. Ryals RC, Andrews MD, Datta S, et al. Long-term characterization of retinal degeneration in Royal College of Surgeons rats using spectral-domain optical coherence tomography retinal thickness in RCS rats acquired with OCT. *Invest Ophthalmol Vis Sci*. 2017;58:1378–1386.

32. Eldred GE, Katz ML. Fluorophores of the human retinal pigment epithelium: separation and spectral characterization. *Exp Eye Res*. 1988;47:71–86.

33. Kennedy CJ, Rakoczy PE, Constable IJ. Lipofuscin of the retinal pigment epithelium: a review. *Eye*. 1995;9:763–771.

34. Ben-Shabat S, Parish CA, Vollmer HR, et al. Biosynthetic studies of A2E, a major fluorophore of retinal pigment epithelial lipofuscin. *J Biol Chem*. 2002;277:7183–7190.

35. Sparrow JR, Duncker T. Fundus autofluorescence and RPE lipofuscin in age-related macular degeneration. *J Clin Med*. 2014;3:1302–1321.

36. Panthier C, Querques G, Puche N, et al. Evaluation of semiautomated measurement of geographic atrophy in age-related macular degeneration by fundus autofluorescence in clinical setting. *Retina*. 2014;34:576–582.

37. Yung M, Klufas MA, Sarraf D. Clinical applications of fundus autofluorescence in retinal disease. *Int J Retina Vitreous*. 2016;2:12.

38. Ly A, Nivison-Smith L, Assaad N, Kalloniatis M. Fundus autofluorescence in age-related macular degeneration. *Optom Vis Sci*. 2017;94:246–259.

39. Bourne MC, Campbell DA, Tansley K. Hereditary degeneration of the rat retina. *Br J Ophthalmol*. 1938;22:613–623.

40. Popescu DP, Choo-Smith LP, Flueraru C, et al. Optical coherence tomography: fundamental principles, instrumental designs and biomedical applications. *Biophys Rev*. 2011;3:155.

41. Altman DG, Bland JM. Measurement in medicine: the analysis of method comparison studies. *Statistician*. 1983;32:307–317.

42. Sparrow JR, Kim SR, Wu Y. Experimental approaches to the study of A2E, a bisretinoid lipofuscin chromophore of retinal pigment epithelium. *Methods Mol Biol*. 2010;652:315–327.

translational vision science & technology